Real-Time Automatic Artery Segmentation, Reconstruction and Registration for Ultrasound-Guided Regional Anaesthesia of the Femoral Nerve

Erik Smistad* and Frank Lindseth

***Abstract*—The goal is to create an assistant for ultrasound-guided femoral nerve block. By segmenting and visualizing the important structures such as the femoral artery, we hope to improve the success of these procedures. This article is the first step towards this goal and presents novel real-time methods for identifying and reconstructing the femoral artery, and registering a model of the surrounding anatomy to the ultrasound images. The femoral artery is modelled as an ellipse. The artery is first detected by a novel algorithm which initializes the artery tracking. This algorithm is completely automatic and requires no user interaction. Artery tracking is achieved with a Kalman filter. The 3D artery is reconstructed in real-time with a novel algorithm and a tracked ultrasound probe. A mesh model of the surrounding anatomy was created from a CT dataset. Registration of this model is achieved by landmark registration using the centerpoints from the artery tracking and the femoral artery centerline of the model. The artery detection method was able to automatically detect the femoral artery and initialize the tracking in all 48 ultrasound sequences. The tracking algorithm achieved an average dice similarity coefficient of 0.91, absolute distance of 0.33 mm, and Hausdorff distance 1.05 mm. The mean registration error was 2.7 mm, while the average maximum error was 12.4 mm. The average runtime was measured to be 38, 8, 46 and 0.2 milliseconds for the artery detection, tracking, reconstruction and registration methods respectively.**

***Index Terms*—Artery segmentation, artery tracking, femoral nerve block, GPU, real-time, regional anaesthesia, ultrasound.**

I. Introduction

THE use of regional anaesthesia (RA) is increasing due to the benefits over general anaesthesia (GA) such as reduced morbidity and mortality [27], [5], [35], reduced postoperative pain, earlier mobility, shorter hospital stay, and lower costs [9]. Despite these clinical benefits, RA remains less popular than GA. One reason for this is that GA is far more successful and reliable than RA. Ultrasound has been employed to increase the success rate of RA [14], [12]. However, ultrasound-guided RA can be a challenging technique, especially for inexperienced physicians and in difficult cases. Good theoretical, practical and non-cognitive skills are needed in order to achieve confidence in performing RA and to keep complications to a minimum. Studies indicate that RA education focusing on illustrations and text alone is not sufficient [36]. The RASimAs[1] project (Regional Anaesthesia Simulator and Assistant) is a European research project which aims at providing a virtual reality simulator to improve the training of doctors performing RA, as well as an assistant to lessen the cognitive burden and help performing RA procedures.

This article focuses on creating an assistant for ultrasound-guided RA to block the femoral nerve. In this application, the femoral artery is an important structure used to locate the femoral nerve [24] as shown in Figs. 1 and 3. A study by Gruber *et al.* [15] showed that in 77.5% of the cases the femoral nerve was located within 5 mm of the femoral artery. The rest were located more than 5 mm lateral of the artery. This article presents novel methods for identifying and reconstructing the femoral artery from ultrasound images, and registering a model of the surrounding anatomy to the images. The idea is that the registered model together with the segmented artery will help locate the femoral nerve. The hypothesis that this assistant helps identifying the femoral nerve is not validated in this article. However, the assistant will be clinically tested and evaluated in future work at three different clinical sites as part of the ongoing RASimAs project. The accuracy of the femoral artery segmentation and model registration is evaluated in this article.

Several methods for segmentation of the cross-section of vessels in 2D ultrasound have been reported, using methods such as level sets [1], fuzzy c-means clustering [2] and evolutionary algorithms [18]. These methods focus on segmenting a single image. However, in this work the goal is to segment the femoral artery in real-time on a sequence of ultrasound images. Abolmaesumi *et al.* [3], [4] and Guerrero *et al.* [16], [17] presented

Manuscript received August 19, 2015; revised October 19, 2015; accepted October 20, 2015. Date of publication October 26, 2015; date of current version March 01, 2016. This project has received funding from the European Union's Seventh Framework Programme for research, technological development and demonstration under Grant 610425. *Asterisk indicates corresponding author.*

*E. Smistad is with the Department of Computer and Information Science at the Norwegian University of Science and Technology and SINTEF Medical Technology, 7491 Trondheim, Norway (e-mail: smistad@idi.ntnu.no).

F. Lindseth is with the Department of Computer and Information Science at the Norwegian University of Science and Technology and SINTEF Medical Technology, 7491 Trondheim, Norway.

Color versions of one or more of the figures in this paper are available online at http://ieeexplore.ieee.org.

Digital Object Identifier 10.1109/TMI.2015.2494160

[1]http://www.rasimas.eu

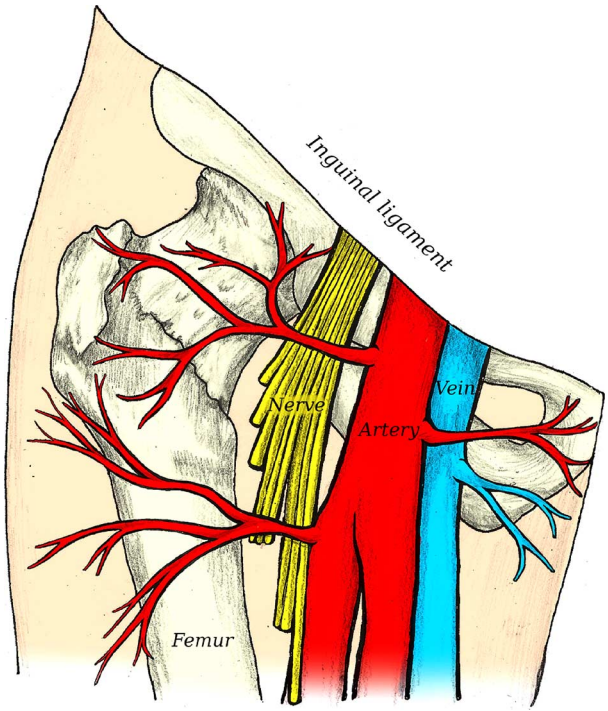

Fig. 1. Illustration of the femoral nerve block region showing the femoral artery, vein and nerve along with femur and the pelvic bone. Image courtesy of H. E. Mørk (helemork.com).

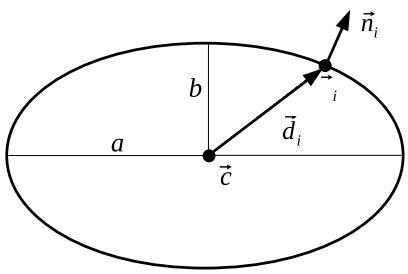

Fig. 2. Artery cross-section modelled as an ellipse with major radius a, minor radius b and center $\vec{c}$.

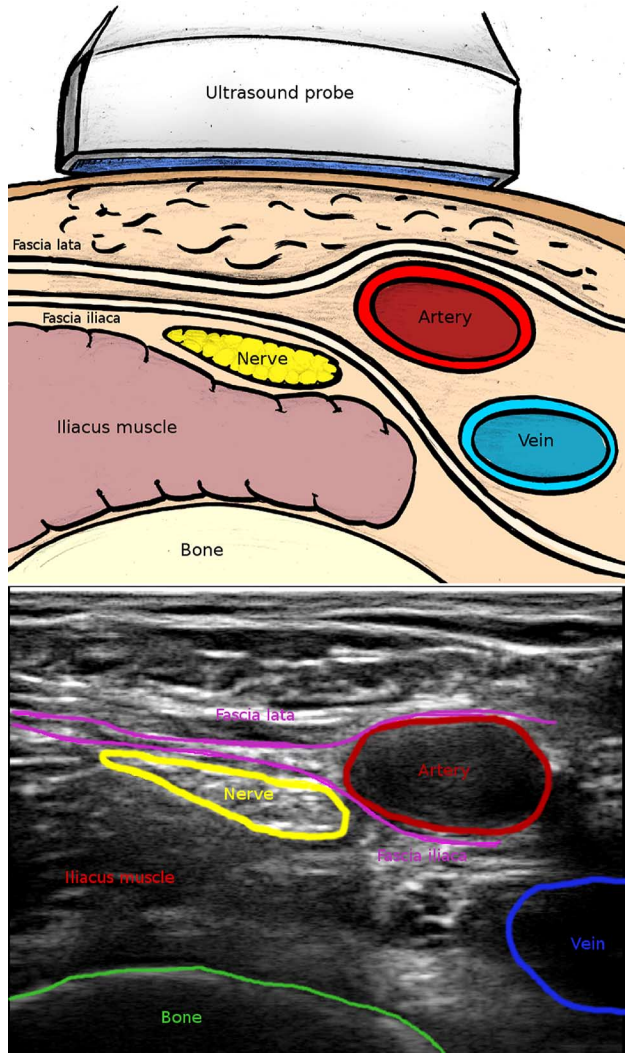

Fig. 3. Top: Cross-section illustration of the region of interest (ROI). Image courtesy of H. E. Mørk (helemork.com) Bottom: Ultrasound image of the ROI with manual annotations delineated by an expert. The image was acquired with an Ultrasonix L14-5 linear probe with harmonic imaging, 6.6 MHz frequency and 55% gain.

methods for vessel segmentation and tracking in ultrasound images using an extended Kalman filter. Their methods were fast and accurate, but had to be manually initialized with a seed point inside the vessel.

The contributions of this article are:

- A real-time automatic artery detection method. This method eliminates the need for manual initialization such as in the methods of Abolmaesumi *et al.* [3], [4] and Guerrero *et al.* [16], [17].
- A real-time vessel tracking method of the femoral artery similar to the approaches of Abolmaesumi *et al.* [3] and Guerrero *et al.* [16], [17]. While their methods use two Kalman filters, one for estimating the position of the vessel and another to estimate the shape, the proposed method uses only one Kalman filter resulting in a simpler method.
- A real-time vessel 3D reconstruction method. Unlike the reconstruction method of Guerrero *et al.* [16], the proposed method can also reconstruct bifurcations.
- A real-time vessel registration method which registers a model of the femoral region anatomy to the ultrasound images. The method is automatic and provides anatomical reference to the operator.

II. Methods

This section first describes the artery model used to detect and track the femoral artery. Next, the artery detection, tracking and 3D reconstruction methods are presented. Finally, the registration method is described. To achieve real-time performance, the presented methods are implemented using the framework for heterogeneous medical image computing and visualization (FAST) [30]. This framework enables efficient computation and visualization on heterogeneous systems which include different processors such as CPUs and graphic processing units (GPUs). GPUs have shown to have great potential in accelerating medical image segmentation [33], registration [13] and visualization [31], [8].

A. Experimental Setup

The experimental setup consisted of an Ultrasonix SonixMDP scanner (Analogic, Boston, USA) together with an L14-5 linear probe and SonixGPS electromagnetic tracking. Spatial calibration was done using a calibration matrix from the manufacturer [34]. Harmonic imaging was used with frequency 6.6 MHz and gain at 55%. The images were streamed from the ultrasound system to the proposed assistant using the Plus toolkit and the OpenIGTLink protocol [22]. The pixel spacing was determined by the Plus toolkit which queries this information directly from the ultrasound system.

B. Artery Model

The artery cross-section in the ultrasound images is modelled as an ellipse with major and minor radii a and b, as shown in Fig. 2. The cross-section of arteries will not necessarily have the exact shape of an ellipse. However, in the application of RA exact delineation of the artery border is not required. The point $\vec{p}_i$ and its normal $\vec{n}_i$ of point i on an ellipse of N points with center $\vec{c}$ can be calculated with the following equations.

$$\alpha_i = \frac{2\pi i}{N} \tag{1}$$

$$\vec{d}_i = [a\cos(\alpha_i), b\sin(\alpha_i)] \tag{2}$$

$$\vec{p}_i = \vec{c} + \vec{d}_i \tag{3}$$

$$\vec{n}_i = \frac{[b\cos(\alpha_i), a\sin(\alpha_i)]}{|[b\cos(\alpha_i), a\sin(\alpha_i)]|}. \tag{4}$$

C. Artery Detection

In this section, a novel fully automatic artery detection method is presented which is used to initialize the artery tracking algorithm described in the next section. First, the image is blurred using convolution with a Gaussian mask ($\sigma = 0.5$ mm) and then the image gradients $\vec{G}$ are calculated. For a given radii a and b, the artery score S is calculated as the average dot product of the outward normal $\vec{n}_i$ and the corresponding image gradient at N points on the ellipse, as shown in (5). Before the dot product is calculated, the image gradient is normalized so that it has unit length. This normalization makes this artery detection method invariant to the contrast of the image, and only the direction of the gradients influence the score.

$$S(\vec{c}, a, b) = \frac{1}{N}\sum_{i=0}^{N-1} \vec{n}_i \cdot \frac{\vec{G}(\vec{p}_i)}{|\vec{G}(\vec{p}_i)|}. \tag{5}$$

For each pixel, ellipses of different major radius a ranging from 3.5 to 6 mm, flattening factor f from 0 to 0.5 (minor radius $b = (1-f)a$) and $N = 32$ samples were used to calculate the artery score. An increment of 0.25 mm was used for the radius, and 0.1 for the flattening factor. The ellipse with the highest score is selected for each pixel. The best score and the values a and b is stored for each pixel. The ellipse with the highest score of all pixels is selected and used to initialize the tracking. Real-time performance of this artery segmentation method is achieved by using a GPU to compute the artery score of all pixels in parallel. This was implemented using FAST and OpenCL.

For a detected artery to be accepted it has to have a artery score S above the threshold $T_s = 0.8$. Also, the centerpoint detected from five consecutive frames has to be within 1.5 mm of each other and the average intensity of the detected artery border has to be above the threshold $T_b = 40$ (gain set to 55%). These requirements are needed to make the artery detection robust enough to properly initialize the artery tracking. They represent a tradeoff between the initialization robustness and how well-defined the artery contour has to be before the tracking is initialized.

D. Artery Tracking

Artery tracking in the ultrasound images is achieved with a Kalman filter [21]. The Kalman filter estimates a state using a set of noisy measurements over time. The state $\mathbf{x}$ consists of 4 variables, the artery center $\vec{c} = [c_x, c_y]$, and the major and minor radii a and b. Thus, the proposed Kalman filter estimates both the position and shape of the artery cross-section which changes over time as new image frames are received. The state is predicted for the next image frame using a motion model [7] as shown in (6), along with the covariance error matrix $\mathbf{P}$ in (7).

$$\bar{\mathbf{x}}_{t+1} = \mathbf{A}_1\hat{\mathbf{x}}_t + \mathbf{A}_2\hat{\mathbf{x}}_{t-1} \tag{6}$$

$$\bar{\mathbf{P}}_{t+1} = \mathbf{A}_1\hat{\mathbf{P}}_t\mathbf{A}_1^T + \mathbf{A}_2\hat{\mathbf{P}}_{t-1}\mathbf{A}_2^T + \mathbf{A}_1\hat{\mathbf{P}}_t\mathbf{A}_2^T + \mathbf{A}_2\hat{\mathbf{P}}_{t-1}\mathbf{A}_1^T + \mathbf{Q}. \tag{7}$$

For the motion model, the velocity of the artery center $\vec{c}$ was dampened by a factor of $d = 0.5$ so that $\vec{c}_{t+1} = \vec{c}_t + (\vec{c}_t - \vec{c}_{t-1})0.5 = 1.5\vec{c}_t - 0.5\vec{c}_{t-1}$. This gives diagonal state transition matrices $\mathbf{A}_1$ and $\mathbf{A}_2$ with values 1.5 and -0.5 respectively for the center coordinate. The radius is not expected to change, therefore the state transition matrix values for the radii a and b was set to 1 and 0. The dampening reduces tracking failure when the artery moves quickly in the image and suddenly stops. A diagonal matrix was also used for the process error matrix $\mathbf{Q}$ with values 0.01. The size of these matrices is equal to the size of the state vector (4×4).

A hybrid edge detection method is used to detect two different types of edges, step edges and ridge edges. The edge detection finds the normal displacement ($v_i = \vec{n}_i^T(\vec{p}_{i,\text{observed}} - \vec{p}_{i,\text{predicted}})$) in a line centered at each point i in the predicted ellipse. The direction of each line is given by the normal vector, and the line length L is set to be equal to the major radius. The hybrid edge detection method first looks for a step edge using a step model [26], which entails finding a k that minimizes the following measure where $l(s)$ is the image intensity at step s along the line.

$$\sum_{s=0}^{k}\left|\left[\frac{1}{k+1}\sum_{j=0}^{k} l(j)\right] - l(s)\right| + \sum_{s=k+1}^{L-1}\left|\left[\frac{1}{L-k}\sum_{j=k+1}^{L-1} l(j)\right] - l(s)\right|. \tag{8}$$

A measurement noise value r_i is also recorded for each edge and is calculated based on the edge strength:

$$r_i = \frac{1}{\frac{1}{L-k}\sum_{j=k+1}^{L-1} l(j) - \frac{1}{k+1}\sum_{j=0}^{k} l(j)}. \quad (9)$$

The step edge is only accepted if the denominator of (9) is above the threshold $T_e = 10$. If the step edge is not accepted, a ridge edge detection is performed. This method looks for the first position s on the line where the gradient is larger than the threshold T_e. If no ridge edge is found either, the measurement for point i is discarded. The measurement noise value for the ridge edges are set to be $r_i = 1/(l(s) - l(s-1))$.

These edge measurements are nonlinear because they cannot be expressed as matrix multiplication of the state $\mathbf{x}$. Therefore an extended Kalman filter is used in which the observation model is linearized. This is done by calculating the Jacobi matrix that relate changes in each ellipse point $\vec{p}_i$ to changes in the state $\mathbf{x}$. The final measurement vector $\vec{h}_i$ is the normal projection of these Jacobi matrices:

$$\begin{aligned}\vec{h}_i &= \vec{n}_i^T \frac{\partial \vec{p}_i}{\partial \mathbf{x}} \\ &= \vec{n}_i^T \begin{bmatrix} 1 & 0 & \cos(\alpha_i) & 0 \\ 0 & 1 & 0 & \sin(\alpha_i) \end{bmatrix}. \end{aligned} \quad (10)$$

By assuming that the measurements are independent, the measurement noise covariance matrix $\mathbf{R}$ becomes a diagonal matrix of the measurement noise values r_i. The multiplications of $\mathbf{R}$, the state-to-measurement transition matrix $\mathbf{H}$ and the measurements $\mathbf{v} = [v_0, v_1, \ldots v_{N-1}]$ becomes a simple summation as shown in (11) and (12) [25]. If no edge is found for a measurement point i, it is omitted in the summations.

$$\mathbf{H}^T\mathbf{R}^{-1}\mathbf{v} = \sum_{i=0}^{N-1} \vec{h}_i^T r_i^{-1} v_i \quad (11)$$

$$\mathbf{H}^T\mathbf{R}^{-1}\mathbf{H} = \sum_{i=0}^{N-1} \vec{h}_i^T r_i^{-1} \vec{h}_i. \quad (12)$$

This formulation avoids matrix multiplications and inversions of large matrices in the Kalman update (13) and (14). As shown by Blake and Isard [6], using $\hat{\mathbf{P}}_{t+1}\mathbf{H}^T\mathbf{R}^{-1}$ as the Kalman gain, the updated state and error covariance estimate becomes:

$$\hat{\mathbf{P}}_{t+1} = (\bar{\mathbf{P}}_{t+1}^{-1} + \mathbf{H}^T\mathbf{R}^{-1}\mathbf{H})^{-1} \quad (13)$$

$$\hat{\mathbf{x}}_{t+1} = \bar{\mathbf{x}}_{t+1} + \hat{\mathbf{P}}_{t+1}\mathbf{H}^T\mathbf{R}^{-1}\mathbf{v}. \quad (14)$$

E. 3D Artery Reconstruction

The ultrasound probe is tracked using the electromagnetic tracking system SonixGPS (Analogic, Boston, USA). This enables 3D reconstruction of the artery tracked in the 2D ultrasound images. Each center coordinate $\vec{c}$ from the artery tracking is converted into a 3D coordinate using the transformation provided by the electromagnetic tracking system. 3D reconstruction is done by adding a sphere to a volume at the 3D coordinate. Finally, a real-time marching cubes algorithm is used to generate a surface mesh of the volume and visualize it as shown in Fig. 4. These steps are all performed for each new tracked centerpoint.

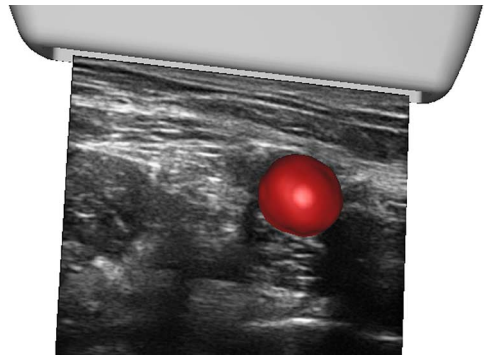

Fig. 4. 3D artery reconstruction. The radius and position provided by the artery tracking method is used to add a sphere to a volume. From this volume, a surface mesh of the femoral artery is generated and visualized together with the current ultrasound image.

A volume of size $256 \times 256 \times 512$ voxels is created and each voxel is initialized to zero. The longest side of the volume is aligned with the femoral artery direction. Using a larger volume would reduce the speed, and using a smaller would reduce the accuracy of the reconstruction. The voxel spacing is set to 0.5 mm, which means that the volume can cover an area of size $12.8 \times 12.8 \times 25.6$ cm which is large enough for the femoral nerve block region. When the artery tracking is first initialized, the transformation of the current ultrasound image T_{US} is used to position and orient the volume. This is done by placing the center of the volume at the center of the artery and using the same orientation as the ultrasound image frame as shown in (15). It is assumed that the probe is placed in the femoral region so that the image plane is approximately aligned with the cross-sectional plane of the femoral artery. The reconstruction volume is only created and positioned once.

$$T_V = T_{\mathrm{US}} * \begin{bmatrix} 1 & 0 & 0 & c_x - \frac{256}{2} \\ 0 & 1 & 0 & c_y - \frac{256}{2} \\ 0 & 0 & 1 & -\frac{512}{2} \\ 0 & 0 & 0 & 1 \end{bmatrix}. \quad (15)$$

The voxel position of the artery centerpoint $\vec{c}$ inside the volume can be calculated as $T_V^{-1} * T_{\mathrm{US}} * [c_x, c_y, 0, 1]^T * (1/0.5\ \mathrm{mm})$. All voxels which are within the radius $(a+b)/2$ of this voxel position are given the value 1. Due to pressure applied by the operator holding the probe, the artery is usually flattened. In the visualization, the goal is to show the artery as if such pressure was not applied. This is why a sphere was chosen instead of an ellipsoid. The volume is then smoothed by convolution with a 3D Gaussian mask with $\sigma = 0.5$ mm. Finally, a surface mesh of the reconstructed volume is generated by a real-time GPU-based marching cubes algorithm [31] and visualized in the 3D scene.

F. Registration

The anatomical model was created from a single abdominal CT image volume with the patient in supine position. From this CT image volume, the bone was segmented using region growing, and the centerline of the femoral artery was extracted

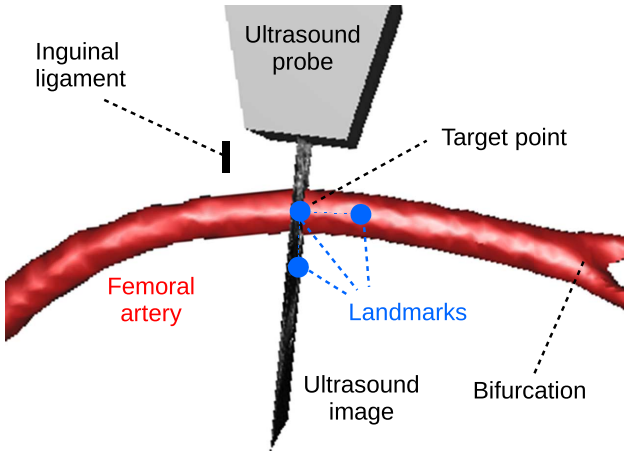

Fig. 5. Landmark registration of the model to the ultrasound images. A target point is determined with the artery tracking using the centerpoint position and radius. Two additional landmarks (blue dots) are created. One in the direction of the artery and one below the artery. A distance of 10 mm from the target point to the other two landmarks is used in this figure for illustration purposes.

using the tubular extraction method of Smistad *et al.* [32]. Ideally, a CT scan of the patient undergoing RA would be used. However, this is not always available, and therefore a single CT image volume is used to create the model. The model and its registration is only used to give the operator an overview of the surrounding bone anatomy in relation to the ultrasound probe and image using a 3D visualization as shown in Fig. 7. Since the model does not incorporate the anatomical variation in this region, the visualization is not expected to be accurate.

Registration of the model to the ultrasound images is difficult as there are no easily identifiable landmarks in the ultrasound images. It would be possible to scan different landmark areas or bones and use this for registration. However, this would involve changing the actual femoral nerve block procedure, which is not desired. The artery tracking method provides the centerpoint and radius for the femoral artery. This is used together with the assumptions and knowledge of the femoral artery anatomy to register the model to the ultrasound images. The femoral artery is a continuation of the external iliac artery, which rises up from the abdomen under the inguinal ligament. At about 3.5–5 cm inferior to the inguinal ligament, the femoral artery gives off to the deep femoral artery and becomes the superficial femoral artery [23]. The target injection site is between the inguinal ligament and this bifurcation as shown in Figs. 1 and 5. The artery centerpoint with minimum depth and within 1 mm of the largest radius is selected as the artery target centerpoint. This is not a unique landmark, and will surely be a source of registration error which is evaluated in this article. The requirement of minimum depth discards all artery centerpoints that are superior to the inguinal ligament, and the largest radius requirement discards artery centerpoints after the bifurcations because the radius generally decreases after the bifurcation. The depth is estimated using the distance from the top of the ultrasound image to the artery centerpoint.

The corresponding target point is identified manually in the model and landmark registration is used to register the ultrasound images to the model. Three landmarks are needed for the registration. To obtain two more landmarks, two points at fixed directions and distances are estimated from the ultrasound images. The second landmark is selected in the direction of the artery 1 mm from the target point. The direction of the artery is calculated using the centerpoints from the artery tracking. The third landmark is 1 mm below the target point as shown in Fig. 5. The directions from the target point to the two landmarks are therefore perpendicular. This insures that only anatomical feasible orientations are generated by the landmark registration. The downwards direction is estimated using the image plane of the initial ultrasound image. This requires the operator to initially hold the probe vertical when placing the probe at the skin. Afterwards, the operator may tilt the probe, a technique which is often required to see all the structures properly in ultrasound. All the corresponding landmarks were identified manually in the CT image volume.

Let $\mathbf{F}$ and $\mathbf{M}$ be the fixed landmarks from the ultrasound image and the moving landmarks of the model respectively. Kabsch's algorithm [20] finds the optimal rotation matrix $\mathbf{R}$ using singular value decomposition, see [10] for details. The complete transformation is calculated in (16) using the centroids $\vec{C}_F$ and $\vec{C}_M$ of the fixed and moving landmarks. The target is updated continuously, and if the target changes, the registration is executed again and the visualization updated.

$$\begin{bmatrix} 1 & 0 & 0 & C_{F,x} \\ 0 & 1 & 0 & C_{F,y} \\ 0 & 0 & 1 & C_{F,z} \\ 0 & 0 & 0 & 1 \end{bmatrix} * \mathbf{R} * \begin{bmatrix} 1 & 0 & 0 & -C_{M,x} \\ 0 & 1 & 0 & -C_{M,y} \\ 0 & 0 & 1 & -C_{M,z} \\ 0 & 0 & 0 & 1 \end{bmatrix}. \quad (16)$$

G. Evaluation

A total of 48 ultrasound image sequences from both legs of 3 male and 3 female subjects were collected using the setup described in Section II-A. The subjects were all in supine position during acquisitions. Initially, the probe was placed below the inguinal ligament. Next, the probe was moved in an area from 2–3 centimeters above the ligament down to the bifurcation where the femoral artery gives off to the deep femoral artery of the thigh. The number of images per sequence ranged from 118 to 740. For each sequence, the artery was manually segmented in 4 randomly selected frames. This resulted in 192 manual segmentations used to evaluate the artery detection and segmentation methods. The dice similarity coefficient D [11] was calculated to measure the overlapping regions of the segmentation S and the ground truth G as shown in (17). For the contour of the segmentation, the mean absolute distance A and Hausdorff distance H was calculated in millimeters. These measures were calculated as shown in (18) and (19), and used to evaluate the artery detection and tracking methods. $\bar{d}(i, G, S)$ is the distance from contour point i in G to the closest contour point in S. O and M are the number of pixels on the contour of G and S respectively.

$$D = \frac{2|S \cap G|}{|S| + |G|} \quad (17)$$

$$A = \frac{1}{2}\left(\frac{1}{O}\sum_{i=0}^{O-1}\bar{d}(i, G, S) + \frac{1}{M}\sum_{i=0}^{M-1}\bar{d}(i, S, G)\right) \quad (18)$$

$$H = \max\left(\max_{i\in[0..O-1]}\bar{d}(i, G, S), \max_{i\in[0..M-1]}\bar{d}(i, S, G)\right). \quad (19)$$

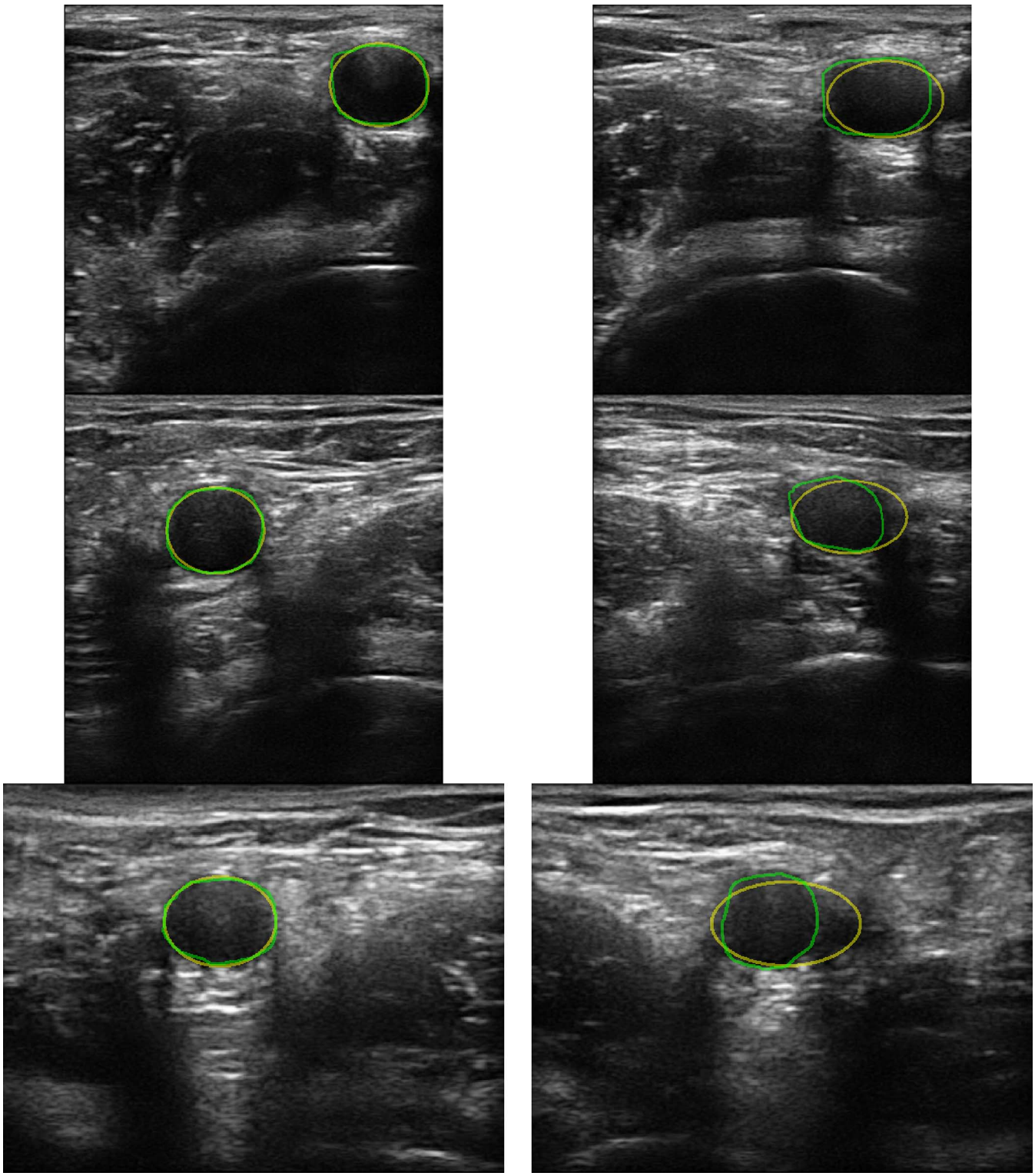

Fig. 6. Best (left column) and worst (right column) segmentation results for three of the subjects determined by the dice similarity coefficient in (17). The green line is the manually segmented artery, while the yellow smooth line is the result of the proposed artery tracking method.

The registration method was evaluated by measuring the distance from each centerpoint $\vec{c}$ obtained with the artery tracking method to the centerline of the registered model. The distance was calculated for the entire extracted centerline, thus for the entire scanned area.

III. Results

The artery detection initialized the tracking successfully in all 48 sequences, and was evaluated separately by executing the proposed algorithm on each of the manually segmented images,

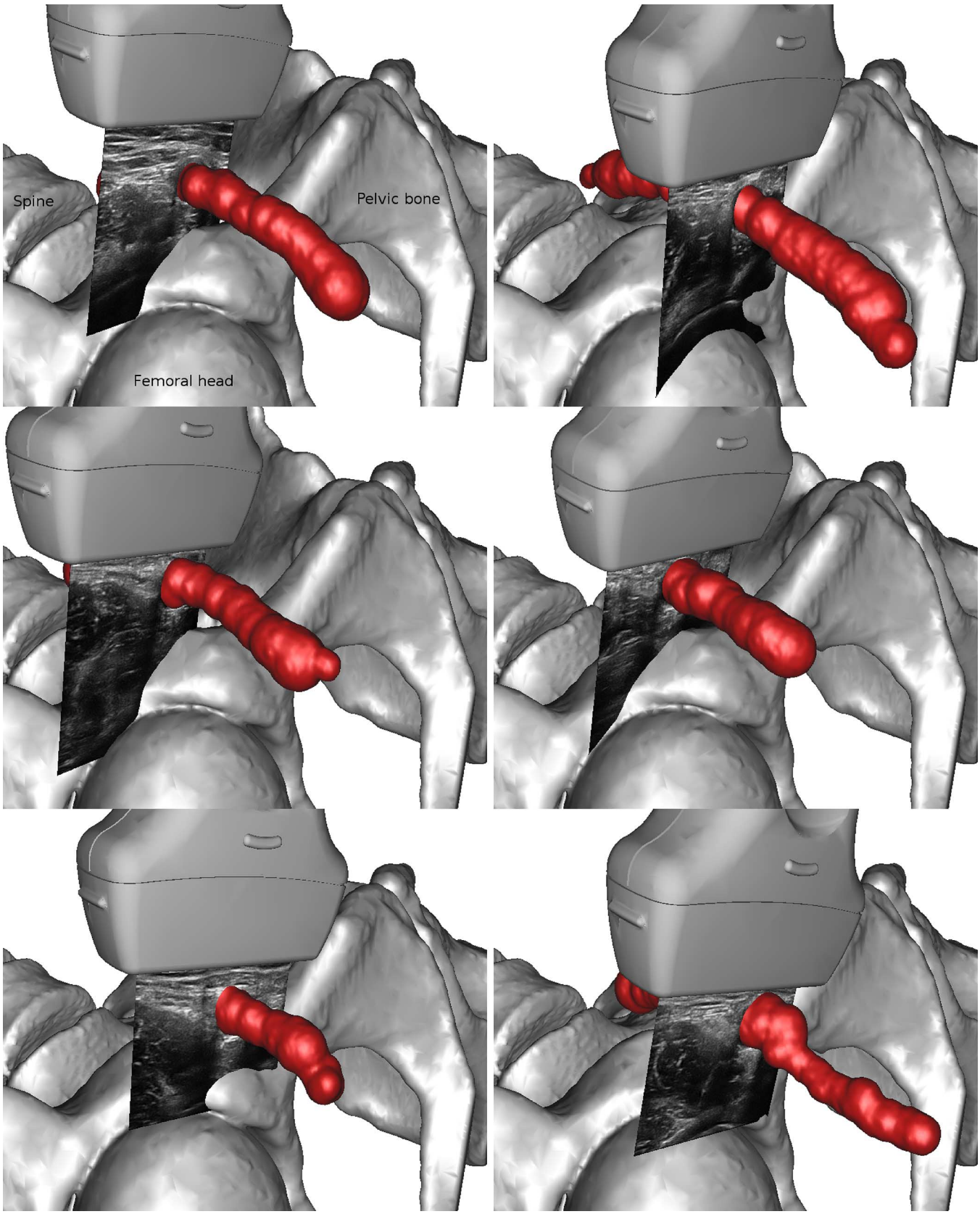

Fig. 7. 3D visualizations for each of the six subjects. The visualization shows the ultrasound probe, ultrasound image, reconstructed femoral artery and the registered bone model.

TABLE I
ACCURACY OF THE ARTERY **DETECTION** USING THE MEASURES IN (17)–(19)

Subject	Mean dice similarity coeff.	Mean absolute distance (mm)	Mean Hausdorff distance (mm)
1	0.89	0.46	1.31
2	0.85	0.57	1.53
3	0.87	0.54	1.63
4	0.86	0.46	1.36
5	0.81	0.66	1.69
6	0.88	0.45	1.17
Average	0.86	0.52	1.45
Std. dev.	0.03	0.08	0.20

TABLE II
ACCURACY OF THE ARTERY **TRACKING** USING THE MEASURES IN (17)–(19)

Subject	Mean dice similarity coeff.	Mean absolute distance (mm)	Mean Hausdorff distance (mm)
1	0.92	0.31	0.98
2	0.94	0.26	0.88
3	0.91	0.39	1.32
4	0.89	0.36	1.09
5	0.90	0.35	1.07
6	0.92	0.30	0.94
Average	0.91	0.33	1.05
Std. dev.	0.02	0.05	0.15

TABLE III
ACCURACY OF THE MODEL TO ULTRASOUND REGISTRATION

Subject	Mean centerline distance (mm)	Max. centerline distance (mm)
1	2.9	12.1
2	2.4	8.4
3	3.1	11.0
4	2.3	14.0
5	2.9	14.1
6	2.5	13.3
Average	2.7	12.4
Std. dev.	0.3	2.2

without the requirement that the artery must be detected at a similar location in five consecutive frames. In 11 of the 192 manually segmented images, the proposed method was not able to detect any artery, and in 4 cases a false artery was detected. Due to the requirement that the artery must be detected at a similar location in five consecutive frames this did not lead to an incorrect initialization. The artery detection method achieved an average dice similarity coefficient of 0.86, mean absolute distance 0.52 mm, and Hausdorff distance of 1.45 mm as shown in Table I.

The results of the artery tracking method for each ultrasound sequence are summarized in Table II. On average, the tracking method achieved a dice similarity coefficient of 0.91, mean absolute distance of 0.33 mm, and mean Hausdorff distance 1.05 mm, after being initialized by the proposed detection method. Images of the best and worst segmentation results, according to D, are shown in Fig. 6 for three of the subjects.

Table III shows the results for the registration error. The average distance between the centerline and the centerpoint of the artery in the ultrasound images was 2.7 mm. The average maximum distance was 12.4 mm. Fig. 7 shows 3D visualizations of the ultrasound probe and image, the reconstructed femoral artery, and the model of the surrounding anatomy after registration for each of the six subjects.

TABLE IV
AVERAGE SPEED IN MILLISECONDS OF PROCESSING ONE FRAME FOR EACH OF THE ULTRASOUND SEQUENCES. NOTE THAT THE ARTERY DETECTION IS ONLY RUN FOR THE FIRST FRAMES, UNTIL THE TRACKING IS INITIALIZED

Subject	Image size	Artery detection	Artery tracking	Artery reconstruction	Artery registration
1	446×460	35.9	8.2	46.3	0.22
2	446×460	35.9	8.5	44.4	0.20
3	446×460	35.8	8.1	44.7	0.18
4	490×382	40.0	6.8	48.3	0.19
5	490×382	38.7	7.1	47.7	0.18
6	490×382	38.9	7.1	45.5	0.18
Average		37.5	7.6	46.2	0.19
Std. dev.		1.9	0.7	1.6	0.01

The runtime of the artery detection, tracking, reconstruction and registration methods was also measured. Table IV contains the average speed of processing one frame of each sequence with the different steps. The computer used to measure the runtime was running Ubuntu 14.04 Linux with an AMD A10 CPU with 16 GB RAM, an AMD Radeon R9 290 GPU with 4 GB RAM, and a solid state drive.

IV. DISCUSSION

The artery detection method was able to automatically detect the femoral artery and initialize the tracking in all 48 ultrasound sequences, while the method of Guerrero *et al.* [17] has to be manually initialized. This is a great benefit to the femoral nerve block assistant application as no user interaction is needed. It has been suggested to use ultrasound Doppler data to initialize vessel tracking [29]. However, enabling Doppler flow on the ultrasound system for the entire image sector reduced the frame rate significantly, and it was not possible to use Doppler with the harmonic imaging frequency used in the femoral nerve block application. Also, visualizing the flow continuously is not part of the normal work flow for these procedures and would distract the operator. Ideally, both Doppler and B-mode data would be used to initialize tracking. The proposed initialization method can easily be extended to use Doppler as well as B-mode data.

Guerrero *et al.* [17] reported a mean error of 1.7 pixels using their method on ultrasound images of the common carotid artery, jugular vein and saphenous vein and artery. They do not report the error in millimeters nor the pixel spacing of their ultrasound data, only the range of pixel spacing for their system (0.069 – 0.2 mm). The mean absolute distance using the proposed method on the femoral artery datasets in pixels is 4, thus worse than the method by Guerrero *et al.* [17]. However, this may partially be due the low pixel spacing of the ultrasound images used in this work (0.079–0.087 mm). Gruber *et al.* [15] reported an average cross-sectional area of 21.7 ± 5.2 mm^2 of the femoral nerve. Sandgren *et al.* [28] measured the average femoral artery radius to be 4.9 mm in male subjects and 4.1 mm in female subjects resulting in an average cross-sectional area of 75 and 53 mm^2. Thus, we argue that the achieved tracking accuracy (mean absolute difference of 0.33 mm) is good in terms of the application of ultrasound-guided femoral nerve block.

The accuracy of the registration was measured using the distance between the centerline of the femoral artery in the model and the centerpoints of the artery tracking. The mean distance was 2.7 mm, while the average maximum distance

TABLE V
A LIST OF PARAMETERS USED IN THE PROPOSED METHODS ALONG WITH A DESCRIPTION OF HOW THEIR VALUE INFLUENCE PERFORMANCE

Parameter	Description	Value used	Possible range
T_e	Edge detection threshold. For an edge detection measurement to be accepted, the edge must be stronger than this value. Lowering it will allow weaker edges (possibly false edges) to be accepted as measurements for the Kalman filter. The value used is low and allow most edges.	10	0 - 255
T_b	Artery detection border threshold. The average intensity along the artery border must be at least this value to be accepted in the artery detection step. Lowering this value will make the detection algorithm accept dark ellipses with low intensity borders. Setting it too high, and the detection will not accept any dark ellipses as arteries.	40	0 - 255
T_s	Artery detection score threshold. The average fit of the inward normals and the image gradient at each sample point on the ellipse (5) must be higher than this value for the artery to be accepted. An artery detection score of 1 is a perfect fit.	0.8	-1 - 1
N	Number of samples to be used for the detection and tracking algorithms. Increasing it may increase accuracy, but will also result in slower runtime as more measurements must be acquired.	32	4 - ∞
$\mathbf{Q}$	Covariance matrix of the process noise. This matrix influences how much the measurements affect the state update in the Kalman filter. Lowering it will make the state update less affected by the measurements and vica versa.	0.01	0 - ∞
d	Dampening factor in the motion model (6). This value determines how much the previous state estimate $\mathbf{x}_{t-1}$ influence the state prediction. Lowering it will decrease the velocity from one frame to another and setting it to 0 will remove the motion completely. If set to 1, the motion model will use constant velocity.	0.5	0-1

was 12.4 mm. Anatomical subject variations of the femoral artery and the artery landmarks are most likely the main causes of the registration error. Currently, a static model of the surrounding anatomy is used, which does not incorporate the anatomical variations seen in a population. However, the model is only used to give the operator an overview of the surrounding bone anatomy. No anatomically invalid orientations were created by the registration, nor were the bone mesh and artery mesh intersecting for any of the acquisitions. Several anaesthesiologists have commented on the registration and visualization, concluding that it looks anatomically feasible and is very promising in terms of assisting the procedure. It was discovered that the maximum error occurs superior to the inguinal ligament at the artery centerpoints farthest away from the target point. An area which is not of great interest for the procedure. A higher maximum error was observed in those subjects with a higher height difference compared to the model. Thus, compensating for the height difference might be a way to reduce the maximum error. Whether the static model is good enough will be evaluated in future work when the final femoral nerve block assistant is clinically tested.

The runtime of the tracking was about 7–8 ms for each image, thus less than the 23 ms reported by Guerrero *et al.* [17]. For the artery detection and reconstruction, the runtime was higher, but still within the real-time constraint of 10–25 frames per second of the ultrasound system. This was achieved with a GPU and the FAST framework. An alternative to the artery reconstruction method of filling a volume and running marching cubes is to draw triangulated ellipsoids. This would be much faster. However, the proposed method was more visually pleasing, enabled smoothing of the reconstruction, and will also enable reconstruction of other non-circular structures in the future, such as the femoral nerve.

The ultrasound images of the first three subjects were acquired with a depth of 4 cm, the rest with a depth of 2.5 cm. This resulted in different image sizes as shown in Table IV. This did not significantly influence the runtime, although the large images had about 18 thousand more pixels. The reason for this is that the artery detection is only executed in the image down to 2 cm. This is also why the runtime for the artery detection is slightly higher for the images acquired with 2.5 cm depth. These images had a lower pixel spacing resulting in more pixels processed. The artery reconstruction is run on a volume of the same size for all subjects and therefore not dependent on the ultrasound image size.

The proposed methods contain several parameters, which values have been determined through experimentation. Table V provides a list of these parameters along with a description of how their value influence the performance of the proposed methods.

Future work includes segmentation of other structures, such as the femoral nerve, fascia lata and fascia iliaca, needle insertion guidance and enhancement of the local anaesthetic after injection. The idea is that the visualization of the ultrasound probe, surrounding anatomy and segmented artery will help locate the femoral nerve and fascias, and guide the needle insertion and anaesthetic injection. It may also be necessary to create a model which incorporates the anatomical differences in a population using methods such as statistical shape models [19].

V. CONCLUSION

The presented methods are able to automatically and accurately track the femoral artery in ultrasound images and use this to reconstruct the artery in 3D and register it to a model of the surrounding anatomy in real-time. The proposed algorithms will be part of an assistant for ultrasound-guided regional anaesthesia of the femoral nerve.

REFERENCES

[1] A. R. Abdel-Dayem, "Level set framework for detecting arterial lumen in ultrasound images," *Proc. Comput. Vis. Med. Image Process.*, pp. 267–272, 2011.

[2] A. R. Abdel-Dayem and M. R. El-Sakka, "Fuzzy C-means clustering for segmenting carotid artery ultrasound images," *Image Anal. Recognit.*, pp. 935–948, 2007.

[3] P. Abolmaesumi, M. Sirouspour, and S. Salcudean, "Real-time extraction of carotid artery contours from ultrasound images," in *Proc. 13th IEEE Symp. Comput.-Based Med. Syst.*, 2000, pp. 2–7.

[4] P. Abolmaesumi and M. R. Sirouspour, "An interacting multiple model probabilistic data association filter for cavity boundary extraction from ultrasound images," *IEEE Trans. Med. Imag.*, vol. 23, no. 6, pp. 772–784, Jun. 2004.

[5] W. S. Beattie, N. H. Badner, and P. Choi, "Epidural analgesia reduces postoperative myocardial infarction: A meta-analysis," *Anesthesia Analgesia*, vol. 93, pp. 853–858, 2001.

[6] A. Blake and M. Isard, *Active Contours: The Application of Techniques from Graphics, Vision, Control Theory and Statistics to Visual Tracking of Shapes in Motion*. London, U.K.: Springer, 1998.

[7] A. Blake, M. Isard, and D. Reynard, "Learning to track the visual motion of contours," *Artif. Intell.*, vol. 78, no. 1–2, pp. 179–212, 1995.

[8] M. Bozorgi and F. Lindseth, "GPU-based multi-volume ray casting within VTK for medical applications," *Int. J. Comput. Assist. Radiol. Surg.*, May 2014.

[9] V. W. Chan *et al.*, "A comparative study of general anesthesia, intravenous regional anesthesia, and axillary block for outpatient hand surgery: Clinical outcome and cost analysis," *Anesthesia Analgesia*, vol. 93, pp. 1181–1184, 2001.

[10] E. A. Coutsias, C. Seok, and K. A. Dill, "Using quaternions to calculate RMSD," *J. Comput. Chem.*, vol. 25, no. 15, pp. 1849–1857, 2004.

[11] L. R. Dice, "Measures of the amount of ecologic association between species," *Ecology*, vol. 26, no. 3, pp. 297–302, 1945.

[12] J. Dolan, A. Williams, E. Murney, M. Smith, and G. N. C. Kenny, "Ultrasound guided fascia iliaca block: A comparison with the loss of resistance technique," *Regional Anesthesia Pain Med.*, vol. 33, no. 6, pp. 526–531, 2008.

[13] O. Fluck *et al.*, "A survey of medical image registration on graphics hardware," *Comput. Methods Programs Biomed.*, vol. 104, no. 3, pp. e45–57, Dec. 2011.

[14] J. Griffin and B. Nicholls, "Ultrasound in regional anaesthesia," *Anaesthesia*, vol. 65, no. Suppl 1, pp. 1–12, 2010.

[15] H. Gruber, S. Peer, P. Kovacs, R. Marth, and G. Bodner, "The ultrasonographic appearance of the femoral nerve and cases of iatrogenic impairment," *J. Ultrasound Med.*, vol. 22, no. 2, pp. 163–172, 2003.

[16] J. Guerrero, S. E. Salcudean, J. A. McEwen, B. A. Masri, and S. Nicolaou, "System for deep venous thombosis detection using objective compression measures," *IEEE Trans. Biomed. Eng.*, vol. 53, no. 5, pp. 845–854, May 2006.

[17] J. Guerrero, S. E. Salcudean, J. A. McEwen, B. A. Masri, and S. Nicolaou, "Real-time vessel segmentation and tracking for ultrasound imaging applications," *IEEE Trans. Med. Imag.*, vol. 26, no. 8, pp. 1079–1090, Aug. 2007.

[18] P. Guzman, R. Ros, and E. Ros, "Artery segmentation in ultrasound images based on an evolutionary scheme," *Informatics*, vol. 1, pp. 52–71, 2014.

[19] T. Heimann and H.-P. Meinzer, "Statistical shape models for 3D medical image segmentation: A review," *Med. Image Anal.*, vol. 13, no. 4, pp. 543–563, Aug. 2009.

[20] W. Kabsch, "A discussion of the solution for the best rotation to relate two sets of vectors," *Acta Crystallographica Sect. A*, vol. 34, no. 6, pp. 827–828, 1978.

[21] R. E. Kalman, "A new approach to linear filtering and prediction problems," *J. Fluids Eng.*, vol. 82, no. 1, pp. 35–45, 1960.

[22] A. Lasso, T. Heffter, A. Rankin, C. Pinter, T. Ungi, and G. Fichtinger, "PLUS: Open-source toolkit for ultrasound-guided intervention systems," *IEEE Trans. Biomed. Eng.*, vol. 61, no. 10, pp. 2527–2537, Oct. 2014.

[23] H. Mamatha, A. S. D'souza, S. Jessica, and S. Suhani, "A cadaveric study on the variations in the origin, course and branching pattern of the profunda femoris artery," *Int J. Curr. Res. Rev.*, vol. 4, no. 19, pp. 137–145, 2012.

[24] K. C. Nielsen, S. M. Klein, and S. M. Steele, "Femoral nerve blocks," *Techn. Regional Anesthesia Pain Manage.*, vol. 7, no. 1, pp. 8–17, 2003.

[25] F. Orderud, "A framework for real-time left ventricular tracking in 3D+T echocardiography , using nonlinear deformable contours and Kalman filter based tracking," *Comput. Cardiol.*, vol. 33, pp. 125–128, 2006.

[26] S. Rabben *et al.*, "Semiautomatic contour detection in ultrasound M-mode images," *Ultrasound Med. Biol.*, vol. 26, no. 2, pp. 287–296, 2000.

[27] A. Rodgers *et al.*, "Reduction of postoperative mortality and morbidity with epidural or spinal anaesthesia: Results from overview of randomised trials," *Br. Med. J.*, vol. 321, pp. 1493–1497, 2000.

[28] T. Sandgren, B. Sonesson, R. Ahlgren, and T. Länne, "The diameter of the common femoral artery in healthy human: Influence of sex, age, and body size," *J. Vasc. Surg.*, vol. 29, no. 3, pp. 503–10, 1999.

[29] C. Schneider, J. Guerrero, C. Nguan, R. Rohling, and S. Salcudean, "Intra-operative "pick-up" ultrasound for robot assisted surgery with vessel extraction and registration: A feasibility study," in *Information Processing in Computer-Assisted Interventions*. New York: Springer, 2011, vol. 6689, LNCS, pp. 122–132.

[30] E. Smistad, M. Bozorgi, and F. Lindseth, "FAST: Framework for heterogeneous medical image computing and visualization," *Int. J. Comput. Assist. Radiol. Surg.*, 2015.

[31] E. Smistad, A. C. Elster, and F. Lindseth, "Real-time surface extraction and visualization of medical images using OpenCL and GPUs," in *Norsk Informatikkonferanse*. Bodø , Norway: Akademika forlag, 2012, pp. 141–152.

[32] E. Smistad, A. C. Elster, and F. Lindseth, "GPU accelerated segmentation and centerline extraction of tubular structures from medical images," *Int. J. Comput. Assist. Radiol. Surg.*, vol. 9, no. 4, pp. 561–575, 2014.

[33] E. Smistad, T. L. Falch, M. Bozorgi, A. C. Elster, and F. Lindseth, "Medical image segmentation on GPUs—A comprehensive review," *Med. Image Anal.*, vol. 20, no. 1, pp. 1–18, 2015.

[34] GPS Data Collection, 2011 Ultrasonix, Jul. 1, 2015 [Online]. Available: http://www.ultrasonix.com/wikisonix/index.php/GPS_Data_Collection

[35] S. C. Urwin, M. J. Parker, and R. Griffiths, "General versus regional anaesthesia for hip fracture surgery: A meta-analysis of randomized trials," *Br. J. Anaesthesia*, vol. 84, no. 4, pp. 450–455, 2000.

[36] B. S. d. Worm, M. Krag, and K. Jensen, "Ultrasound-guided nerve blocks—Is documentation and education feasible using only text and pictures?," *PLoS ONE*, vol. 9, no. 2, 2014.